CHEMISTRY
A EUROPEAN JOURNAL

DOI: 10.1002/chem.200903148

Reversible Coordination of Dioxygen by Tripodal Tetraamine Copper Complexes Incorporated in a Porous Silica Framework

Clément Suspène, Stéphane Brandès, and Roger Guilard*[a]

Abstract: The present study reports the synthesis and rational design of porous structured materials by using a templating method. A tetraethoxysilylated tripodal tetraamine (TREN) was covalently incorporated in a silica framework with a double imprint: A surfactant template and a metal ion imprint. The presence of a cationic surfactant (CTAB) endowed the material with a high porosity, and the tripodal or square-pyramidal topology of the ligand was preserved thanks to the use of the silylated Cu^{II} complex. After removal of the surfactant and de-metalation, the incorporated tetraamine was quantitatively complexed by $CuCl_2$ and the material has shown after thermal activation that a reversible binding of O_2 on the metal ions occurred. This chemisorption process was monitored by UV/Vis and EPR spectroscopies, and the $Cu:O_2$ adduct was postulated to be an end-on μ-η^1:η^1-peroxodicopper(II) complex bridged by a chloride ion. The Cu^I-active species, formed during the activation step, were fully recovered during several O_2 binding cycles. The high reactivity of the copper complexes and the room-temperature stability of the dioxygen adduct were explained by the fine adaptability of the tripodal ligand to different geometries, the confinement of the active sites in the hybrid silica that protect them from degradation by a control of the metal-ion microenvironment, as well as the short-range lamellar order of the copper complexes in the framework.

Keywords: copper · dioxygen binding · N ligands · organic–inorganic hybrid composites · porous materials

Introduction

Copper metalloenzymes involved in many biological processes have attracted great interest within the scientific community and many studies have been carried out to better understand the mechanisms involved in these biological systems.[1–4] The study of multicopper oxidases revealed cooperativity between two or more copper ions in the activation of dioxygen.[5] The active site in these metalloenzymes comprises copper(I) complexes, which interact with dioxygen and hence play a major role in the oxidation of various biosubstrates. The well-characterized copper oxygenases are catechol oxidase,[6] ascorbate oxidase, tyrosinase,[7] or peptidylglycine α-hydroxylating monooxygenase (PHM).[8] In contrast, haemocyanin is the only copper metalloenzyme able to carry dioxygen, thanks to its active dinuclear complex, and has been one of the most studied copper metalloenzymes since the beginning of the 1970s.[9,10] The dioxygen coordination at room temperature was investigated by many spectroscopic methods,[10,11] which revealed oxidation of copper(I) to copper(II) and formation of a μ-η^2:η^2-peroxodicopper(II) adduct, with a copper–copper distance of 3.6 Å. So far, many studies have been devoted to mimicking the active site structure, spectroscopy, and function of copper metalloenzymes,[12,13] and extensive modeling of their reactivity towards O_2 by using lower molecular weight copper complexes has also been studied.[12–17] These models provide a better understanding of the biological molecules by tuning the steric and electronic environment of the metal ion and have allowed the development of new homogeneous catalysts for selective oxidations under mild conditions. The mimicking models are mostly tripodal polynitrogen ligands that are able to complex copper at different oxidation states and can coordinate molecular oxygen to copper(I) to form copper dioxygen adducts of several types.[7,12,13] The first example of a structurally characterized peroxodicopper complex was obtained by Karlin and co-workers by reaction of $[Cu(tmpa)(CH_3CN)]PF_6$ (tmpa = tris[(2-pyridyl)methyl]-amine) with O_2 at low temperatures (−80 °C).[18,19] Thenceforth, reactivity of various copper(I) tripodal polyamine

[a] C. Suspène, S. Brandès, Prof. R. Guilard
Institut de Chimie Moléculaire de l'Université de Bourgogne
UMR 5260, CNRS, Université de Bourgogne
9 avenue Alain Savary, 21078 Dijon Cedex (France)
E-mail: roger.guilard@u-bourgogne.fr

Supporting information for this article is available on the WWW under http://dx.doi.org/10.1002/chem.200903148.

complexes with dioxygen has been investigated and many of the peroxocopper or superoxocopper complexes formed were only stable at low temperatures.[20–23] Among all the ligands investigated to mimic the dioxygen transport in haemocyanin, the derivatives of tris(2-aminoethyl)amine (TREN) are of particular interest and considerable progress has been made towards to stabilizing O_2 adducts close to room temperature. The X-ray structure of a μ-η^1:η^1-peroxodicopper(II) species was obtained at 193 K starting from a TREN N-functionalized by three benzyl groups.[24]

Recently, a Cu^I complex of a TREN derivative bearing three tetramethylguanidine groups was found to coordinate reversibly dioxygen at 193 K by forming an end-on η^1-superoxocopper adduct.[22,23] Schindler et al also described a μ-η^1:η^1-peroxo Me_6TREN complex that was stable at room temperature and in the solid state, but not in solution.[25] Although these two latter oxygenated species are the most stable described to date, there is a paucity of examples of biomimetic models capable of coordinating molecular oxygen reversibly at room temperature.[26–29] Warming oxygenated species generally causes their decomposition to Cu^{II} complexes through processes involving oxidation or ligand dealkylation.[13,30,31] Hence, most of them were only stable for a few minutes or a few hours, and their regeneration was not possible more than once.

Incorporation of such species into silica-based organic–inorganic hybrids is very attractive for various applications, such as gas binding,[32–35] because the complexes immobilized within the material are expected to be more stable than the analogous ones in solution by avoiding degradation of the active species. These materials can combine the properties of the rigid and porous inorganic framework with the intrinsic reactivity of the functional groups or complexes incorporated into the silica framework. Among the wide diversity of silica hybrids, polyamine-functionalized materials with tetraazacycloalkanes are of particular interest, owing to their remarkable ability to strongly bind transition-metal ions and heavy-metal cations.[36,37] Contrary to materials for which tetraazamacrocycles, such as cyclam, are tethered onto the silica surface by covalent grafting or by sol–gel synthesis,[32,38–42] copolycondensation of tetraalkoxysilylated cyclams gave functionalized silica incorporating cyclic polyamines[43–45] into their framework, and these hybrid solids have shown different and sometimes unusual coordination properties compared to their analogues in solution.[35,46] In recent work,[35] we have shown that the incorporation of tetraazamacrocycles like cyclam in silica matrices by a sol–gel process gave materials able to complex copper(II) salts. After thermal activation, copper(II) to copper(I) reduction occurred, and coordination of dioxygen took place at room temperature with a good affinity and a high selectivity over dinitrogen and carbon monoxide. The chemisorption of dioxygen on the metal ions in the solid state was attributed to a short-range organization of organic receptors in the materials. The major drawback of these materials was the instability of the xerogel texture and the irreversible oxidation of some of the Cu^I complexes, which reduced the number of active sites by one half between two successive oxygenation/deoxygenation cycles. Although the thermodynamic stability of tripodal copper complexes is lower than for cyclam copper complexes ($\log K = 18.5$ for the TREN complex[47] and $\log K = 28.1$ for the cyclam complex[36]), owing to the noncyclic nature of the tripodal ligands, the flexibility of TREN derivatives appears to offer a good opportunity for dioxygen coordination in the solid state, as it allows stabilization of the copper ions in both the +I and +II oxidation states.

Functional groups can also be incorporated in more organized frameworks by using the periodic mesoporous organosilicas (PMOs) concept thanks to surfactant-templated supramolecular assembly.[48–51] These materials are a class of hybrid mesoporous material, in which the organic component is homogeneously and covalently incorporated into the wall of the silica framework,[52–55] and they have attracted considerable attention owing to the large range of potential applications in the field of catalysis, gas or metal ion adsorption, sensors, and optical devices.[55] Thenceforth, a huge number of PMOs were prepared with rigid organic groups such as benzene,[56,57] biphenyl,[58,59] or ethylene,[60] but less is known about PMOs functionalized in their framework by linear[51,61–65] or cyclic polyamine,[43–45,66] or other chelating agents.[67] The few complexation studies of PMOs functionalized by polyamines, such as cyclam,[35,44,45,66] or linear amines[61,62,65,68] reveal very promising results. However, to date the tripodal TREN amine has never been incorporated into the framework of hybrid silicas.

The concept behind these functionalized materials was to prepare supramolecular systems with a very precise environment at the molecular level that controls their structural properties and their reactivity. The incorporation of active complexes should create more or less hydrophobic open spaces in which there are localized functionalities, and these cavities are able to protect their catalytic sites,[69] as for metalloenzymatic systems. Such bioinspired materials are mostly devoted to mimicking the coordination chemistry of the metal center to better understand the effect of the molecular environment on their reactivity, or in contrast to induce unexpected activities never described for such tripodal complexes in solution. One outstanding challenge is thus to develop organic–inorganic hybrids with unexpected properties. However, few studies have reported correlations between coordination chemistry, hydrophobicity, and the confinement effect of the active sites, but it has been shown that it is possible to combine at the same time metal-coordination control and the effect of confinement or hydrophobicity, to modify the catalytic activities and the metal-ion-binding properties.[70–73] Moreover, their properties can be tuned by the nano-organization of the active species, and unusual properties could arise by incorporation of the chelating units into the inorganic framework owing to the short-range arrangement of the organic moieties.[74,75] Thanks to the long-range periodicity of mesostructured templated silicas, PMOs are very useful for embedding polyamine into the framework while keeping the integrity of the

functionalization during the synthetic steps in the preparation of the material.

The present study reports on the rational design of such materials for which a bioinspired copper complex is covalently immobilized in the framework of a hybrid silica in order to stabilize the metal ion in different oxidation states, which should be required to fully recover the active sites through O_2 binding cycles. Herein we describe the reversible coordination of dioxygen at room temperature by tripodal copper complexes incorporated into porous organosilica, which mimics the dioxygen transport in copper-metalloenzyme, such as haemocyanin. It is shown that both the control of the stereochemistry of the complexes incorporated into the silica framework and their confinement in the hybrid solid are required to stabilize the copper–dioxygen adducts at room temperature.

Results and Discussion

Synthesis of the precursors and materials: The tripodal TREN derivatives and the copper(II) complex used to synthesize the functionalized materials were prepared according to Scheme S1 in the Supporting Information. Starting from the tetraamine, the triacetamide TREN **1** was obtained by the action of acetic anhydride in refluxing acetic acid. The three amide functions were reduced in a second step by lithium aluminum hydride in tetrahydrofuran. The distilled Et_3TREN compound **2** was obtained in 58% yield.[76] The addition of 3-iodopropyltriethoxysilane to **2** provided the silylated ligand **L** in 89% yield after refluxing in acetonitrile under argon. The tripodal copper complex precursor [Cu(**L**)Br]Br was synthesized in a last step by complexation with copper(II) bromide under anhydrous conditions. $CuBr_2$ was chosen instead of $CuCl_2$ to avoid a mixture of chloride and bromide ion during the preparation of the material, since bromide was supplied by the cetyltrimethylammonium bromide (CTAB) surfactant used.

Tetraamine-functionalized materials were synthesized in basic medium in the presence of the cationic CTAB surfactant to endow the hybrid solid with enhanced porosity and maintain the structure of the ligand. Notably, the use of a polysilylated ligand, which has its hydrolyzable functions held apart from each other often leads to solids that are functionalized inside their framework and not in the pores.[44,66] Contrary to the macrocycles whose conformation is preserved from solution to the solid state,[35,46] the structure of TREN derivatives is obviously modified during each synthetic step, owing to their linear structure and geometric constraints resulting from the polycondensation reactions occurring during the sol–gel process. Thus, the tripodal topology of the ligand is not preserved in the sol–gel material. This problem should be solved by stabilizing the tripodal topology of the ligand by using the tripodal copper(II) complex as a precursor. The use of this metallic imprinting method should preserve the tripodal arrangement of the ligands from solution to the inorganic solid. Hence, the preparation of porous materials incorporating TREN with a fine control of the stereochemical properties of their copper(II) complexes requires the use of a double imprinting method: the porosity and structuration is induced by the surfactant template and the tripodal geometry of the immobilized complexes is maintained by the metal ion. This concept was previously described in the literature for PMOs in the case of copper(II),[62,77] cadmium(II),[78] and lanthanide complexes.[79] Moreover, the instability of $[Cu(TREN)X]^+$ complexes[47] at pH values lower than 4 prevented us from using such a tripodal precursor for sol–gel reactions in structuring conditions employing the well-known triblock copolymer Pluronic 123 as the surfactant,[51,80,81] as the synthetic conditions required more or less diluted strong acids. These latter ones are considered to play a key role in the assembly of the surfactant and silica precursor through a $N^0H^+X^-I^+$ type interaction in which N^0 is the neutral surfactant,[82,83] X^- is the counteranion, and I^+ is the protonated silicate species. For this reason, we have chosen to synthesize porous hybrid solids incorporating TREN ligands using CTAB as structure-directing agent, as it is well known to provide structured materials in basic conditions.[50,51]

The synthesis of the hybrid materials is described in Scheme 1. A solution containing the tripodal copper complex [Cu(**L**)Br]Br and ten equivalents of tetraethoxysilane (TEOS) was hydrolyzed in the presence of CTAB in basic aqueous media (NaOH). Optimized conditions were found with a molar ratio of Si/CTAB/NaOH/H_2O equal to 1:0.15:0.45:160 that gave a material with a high specific surface area, **M1**. Polycondensation occurred over one hour at room temperature and three days at 353 K. The extraction of the surfactant in acidified refluxing ethanol with hydrochloric acid (1 M) led also to a complete decomplexation of the material, in line with the instability of the tripodal complexes in acidic conditions. The amines were then deprotonated with a twofold excess of triethylamine in ethanol during a short time (20 min) to avoid silica dissolution or destructuration. The deprotonation step was required to allow a nearly quantitative complexation of the immobilized ligands by a copper(II) salt.

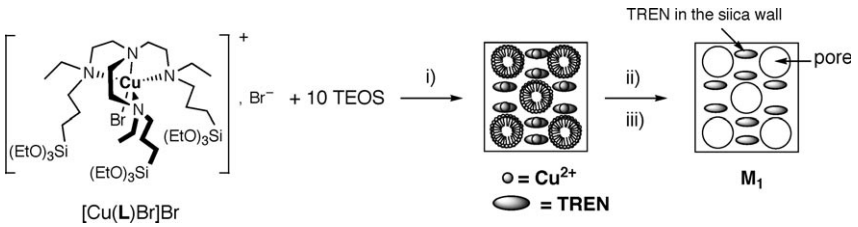

Scheme 1. i) CTAB, 10 equiv TEOS, NaOH, H_2O; ii) HCl/EtOH (1 M); iii) EtOH, Et_3N. 83% overall yield.

To validate the concept of double printing, we have also prepared a material (**M2**) from the free tripodal ligand instead of the [Cu(**L**)Br]Br complex. **M2** presents the same molecular formula as **M1** and was formed under similar experimental conditions.

Structural and textural characterization: The nitrogen adsorption isotherms at 77 K of **M1** (see Figure S1 in the Supporting Information) and **M2** materials are of type I according to the IUPAC classification[84] and are characteristic of a microporous material. According to the BDDT classification,[85] the small hysteresis also indicates the presence of a weak proportion of mesopores. Textural parameters and ligand concentrations of these porous materials are listed in Table 1, and the isotherms give a quite broad pore-size distribution with pore-size diameter lower than 30 Å, according to the BJH calculations.[86] A high specific surface area was determined for **M1** that reveals the efficiency of the surfactant as a structuring and a porogen agent. Material **M2** exhibits lower specific area and pore volume than **M1**, which demonstrates the influence of not only CTAB to create porosity, but also of the copper complex precursor [Cu(**L**)Br]Br. To further confirm the porogen effect of CTAB, a blank material prepared starting from TEOS and [Cu(**L**)Br]Br without using surfactant was shown to be not porous at all. Moreover, in contrast to **M1**, removal of surfactant in the case of mesoporous materials functionalized by diethylenediamine led to matrix collapse, and the resulting extracted materials were disordered and showed low surface areas and small pore volumes.[62]

Table 1. Textural data for **M1** and **M2** materials.

Material	S_{BET}[a] [$m^2 g^{-1}$]	D_p[b] [Å]	V_p[c] [$cm^3 g^{-1}$]	C/N[d]	C/Si[d]	[**L**] ([Cu])[d] [$mmol g^{-1}$]
M1[f]	489	<30	0.29	4.75 (5.20)[e]	0.91 (0.85)[e]	0.82
M1 CuCl$_2$[g]	296	<30	0.17	4.71 (4.78)[e]	0.75 (0.75)[e]	0.74 (0.76)
M2[h]	210	<30	0.13	4.71 (5.32)[e]	–	0.83
M2 CuCl$_2$[g]	161	<30	0.10	4.45 (4.50)[e]	0.74 (0.69)[e]	0.67 (0.81)

[a] Surface are calculated following the BET theory. [b] Pore size diameter obtained from the BJH method. [c] Total pore volume measured at $P/P_0 = 0.99$. [d] Determined from elemental analyses. [e] Theoretical values. [f] Synthesized by using the metal complex imprinting method. [g] Material complexed under argon atmosphere. [h] Synthesized without imprinting metal method.

The composition of the materials was inferred from the results of C, H, N, and Si elemental analyses. The ligand concentration was calculated to be 0.82 and 0.83 $mmol g^{-1}$ for **M1** and **M2**, respectively. The experimental and theoretical C/Si and C/N molar ratios were compared (Table 1) and showed few discrepancies that were mainly attributable to a small amount of CTAB remaining in the solids despite acidic washings. However, this surfactant residue was almost totally removed after copper complexation.

The ^{29}Si and ^{13}C CPMAS NMR spectra for **M1** are presented in Figure S2 in the Supporting Information. Materials **M1** and **M2** were formed with a high degree of polycondensation, as the ^{29}Si NMR spectrum displayed mainly T^3 and Q^4 substructures. The T^n signals are indicative of the incorporation and high condensation of the organosilane derivative within the inorganic silica.

The ^{13}C CPMAS NMR spectrum of **M1** (see Figure S2 in the Supporting Information) displays three broad signals ($\delta = 51.7$, 21.7, 12.7 ppm), which are assigned to the propyl, ethyl, methyl, and ethylene spacers of the ligand. These aliphatic groups present quite similar resonance signals, which explains the broad spectrum observed. The ^{13}C NMR spectrum is thus consistent with the integration of the ligand into the silica framework without alteration.

Although **M1** and **M2** do not exhibit a long-range organization like other PMOs,[48,50,59,87] X-ray diffraction analyses provided information about the nanometer scale organization displayed inside the walls of the silica network, as shown in Figure 1. The X-ray diffraction diagram corresponding to **M1** exhibited only broad diffraction peaks and no sharp Bragg reflection, which indicates the absence of crystalline periodicity. The broad peak (100) centered at 5.9° as well as the second-order broad and weak peak (200) at 11.6° correspond to distances equal to 14.9 and 7.6 Å, respectively, and are characteristic of a lamellar structure with a 14.9 Å interlayer spacing. This distance is attributed to the average length of the organic parts. The presence of these peaks indicates a short-range order in the framework and a quite regular repartition of the

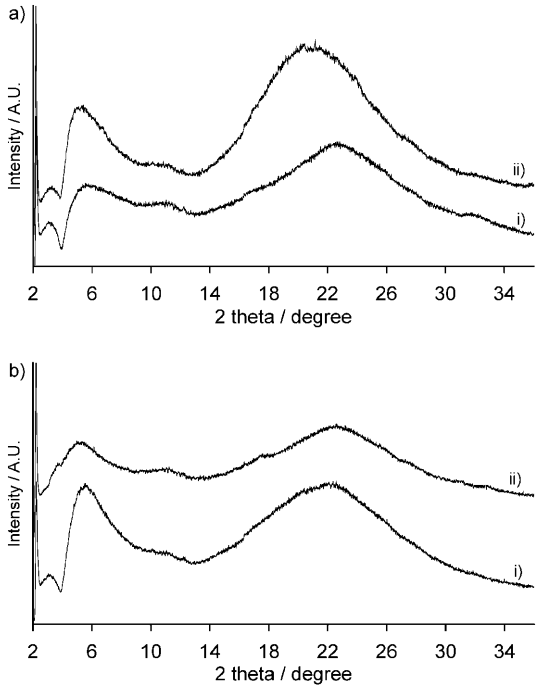

Figure 1. XRD powder diagrams for a) i) **M1** and ii) complexed material **M1 CuCl$_2$** after exposure to O_2; b) i) **M2** and ii) complexed material **M2 CuCl$_2$** after exposure to O_2.

ligand.[75,88–91] It is clear that the organization is not well defined in the long range, as for silylated aryl or long alkyl chains, but such broad signals correspond unambiguously to the existence of a nanometric-scale order in the solid.[59,87,92–96] The peak centered at 23° is related to polyamine chains packing within the layers through the siloxane bonds and represents a 3.9 Å spacing. Therefore, this distance gave an estimation of the closest TREN chelate in the framework.

The X-ray diffraction diagram is similar for **M2** with an interlayer distance of 15.2 Å. However, the sharper peak centered at 5.8° (Figure 1b) indicates a more regular distribution of the organic moieties in the silica network for **M2** than for **M1**, which means a better self-assembly. This can be explained by an extended topology adopted by the free TREN ligand in the case of the formation of **M2**, contrary to a more constrained and folded geometry adopted by the complexed tetraamine during the formation of **M1**. Despite the bowl shape of the tripodal copper complex used to synthesize **M1**, this precursor is able to induce a self-organization on the nanometric scale. Other unfavorable topologies of the silylated reactants have already been shown to provide short-range organization with a precursor possessing tetrahedral geometry.[97]

Reactivity of the copper complexed materials towards O_2 and CO: Materials **M1** and **M2** were metalated in a glove box with copper(II) chloride in dried ethanol under an argon atmosphere and their color changed from white to clear brown before exposure to dioxygen. The complexed materials **M1**$\,$**CuCl$_2$** (see Figure S1 in the Supporting Information) and **M2**$\,$**CuCl$_2$** exhibited a type I nitrogen adsorption isotherm at 77 K comparable to that of **M1** and **M2**, thus indicating that the microporosity of the materials was preserved during metalation. However, textural parameters (Table 1) have shown a significant decrease of the surface areas and pore volumes, as a result of a partial plugging of the pores by the counter-anions. The total amount of copper and TREN moieties incorporated within the hybrid materials was determined by elemental analyses (Table 1). The comparison between both analyses indicated that the metal ion was quantitatively complexed by the immobilized tetraamines and showed the high accessibility of the tripodal ligand to metallic cations in the silica walls.

After an activation step by heating at 393 K under 10^{-3} Torr, **M1**$\,$**CuCl$_2$** and **M2**$\,$**CuCl$_2$** were submitted to several oxygenation/deoxygenation cycles at 295 K under static conditions. The reactivity of these solids towards O_2, CO, and N_2 is depicted in Figure 2 and Table S1 in the Supporting Information. During exposure to O_2, the solids changed from light brown to green, indicating the formation of Cu^{II} ions. As previously described for cyclams incorporating xerogels,[35] the dioxygen reactivity of the material is attributed to copper(I), which is formed by reduction of copper(II) during the activation step. Analysis by using UV/Vis and EPR spectroscopies reveals evidence of this process (see below).

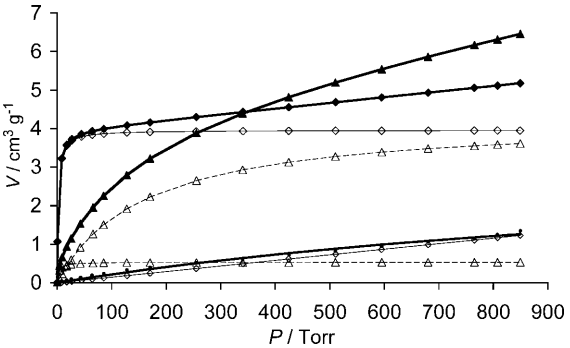

Figure 2. Adsorption isotherms of **M1**$\,$**CuCl$_2$** for O_2 (◆), CO (▲) and N_2 (●) at 295 K. The thin solid lines (◇) are related to chemisorption (Langmuir-type) and physisorption (Henry-type) for O_2 adsorption, and dashed lines (△) indicate the chemisorption contributions for the calculated CO isotherm (see the Experimental Section).

The O_2 experimental adsorption isotherms were analyzed by using a multiple-site adsorption process involving a two Langmuir-type adsorption model (see the Supporting Information).[98–100] This model was required to describe systems with physical and chemical adsorption processes, that is with heterogeneous energetic adsorption sites. Experimentally, we have used a model based on one Langmuir and one Henry isotherm (Figure 2), as the second component of the model has a very low K_2 affinity constant. Similar calculated isotherms were previously described by us for different kinds of materials.[32–35] The first component of a multisite Langmuir isotherm is related to chemisorption of O_2, as it reflects the highest energetic interactions, whereas the second component represents the physisorption process with low energetic interactions and non-selective adsorption by the silica matrix. As N_2 cannot interact with the metal complexes and is only adsorbed by the porous solid through non-selective physisorption, a single Langmuir model was applied to analyze the adsorption isotherm of N_2.

The equilibrium constants for O_2 binding, defined by $K_i = 1/(P_{1/2})_i$, and the adsorption capacity, V_i, were thus calculated and reported in Table S1 in the Supporting Information. Material **M1**$\,$**CuCl$_2$** exhibited a moderate adsorption capacity of O_2 with a volume V_1 of 3.95 $cm^3 g^{-1}$, but a high affinity illustrated by a half saturation pressure $(P_{O_2})_{1/2}$ equal to 2 Torr. The contribution of the physisorption is low since the capacity is only 1.11 $cm^3 g^{-1}$ at 760 Torr, which represents only 22% of the total amount adsorbed. Moreover, it seems reasonable that the physisorption contribution is similar to the N_2 isotherm, the latter being a pure physisorption process. These results clearly point out that O_2 adsorption implied a chemisorption process, which represents the main contribution of the adsorption and is in accordance with the high affinity and selectivity versus N_2. The reactivity of the non-imprinting **M2**$\,$**CuCl$_2$** material was rather similar to that of **M1**$\,$**CuCl$_2$**, but with a slightly lower capacity ($V_1 =$ 3.57 $cm^3 g^{-1}$) and affinity ($(P_{O_2})_{1/2} = 4$ Torr). However, theses differences are too small to attribute them to a beneficial effect of the metal ion imprint by considering only these pa-

rameters. For these two materials, the percentage of active sites, calculated from V_1 and the copper concentration, was far from being complete (around 50%) if we consider the formation of Cu-O_2-Cu dinuclear complex, since only 23.2% of copper ions for **M1CuCl$_2$** for and 19.7% for **M2CuCl$_2$** were involved in O_2 binding. This means that at least one-half of the copper complexes did not coordinate O_2.

The most convincing explanation to interpret this result lies in the inhomogeneous copolycondensation of the silylated TREN precursor with 10 equivalents of TEOS, despite the use of a surfactant, which should induce the structuration of the material and a regular dilution of the organic moieties into the silica.[101] The inhomogeneous incorporation of the organic moieties affords a material in which some of the complexes are in close proximity and have moderate to strong interactions, and some of which are isolated from each other. This propensity for the aggregation of organic moieties during the copolycondensation of a bridged precursor and TEOS was previously observed for xerogels in the absence of surfactant.[74,102] These results are thus in agreement with the dilution of the ligand in a locally lamellar structure. For copper–xerogels incorporating cyclam,[35] the dilution of the active sites in the matrix using TEOS as a silica precursor led to a significant decrease of the percentage for O_2 binding to copper, because of the lack of reactivity of the most isolated copper sites. Thus we can assume that the active sites are mainly dicopper complexes in close interaction; these allow the formation of μ-peroxo species (Scheme 2).

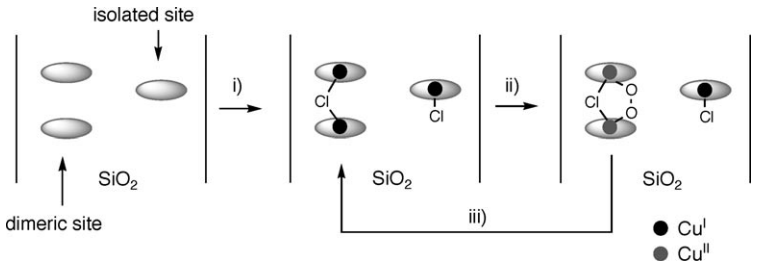

Scheme 2. i) $CuCl_2$, dried EtOH under argon atmosphere, then thermal activation under vacuum; ii) O_2; iii) deoxygenation by heating the material under vacuum.

The reversibility of the oxygenation reaction was studied for **M1CuCl$_2$** and **M2CuCl$_2$** through five oxygenation/deoxygenation cycles at 295 K (see Figure S3 in the Supporting Information). After the sample was degassed for 3 h, the color of the solid changed systematically from green to light brown, and inversely after exposure to O_2. These color changes depict the redox process of copper, namely the reduction of Cu^{II} to Cu^{I} after removing O_2. A reversibility of 97% was indeed deduced from the values of V_1 for the second, third, and fourth cycles of oxygenation/deoxygenation (see Table S2 in the Supporting Information). Moreover, a reversibility of 81% was determined after the material was exposed to moist air over two weeks. This unprecedented reversibility is far higher than the 50% found for the xerogels incorporating tetraazamacrocycles.[35] Another important point is the lower reversibility for O_2 binding displayed by **M2CuCl$_2$** and the lower stability of the texture through O_2 cycles. These results show that metal imprinting of the tripodal copper complexes is required to induce a high reactivity towards O_2 and stability of the dioxygen adducts.

The reactivity of **M1CuCl$_2$** and **M2CuCl$_2$** towards CO was also studied and the results are reported in Table S1 in the Supporting Information and Figure 2. CO can be considered as a redox probe of copper, as it should coordinate only to the Cu^{I}. However, the affinity was higher for O_2 than for CO, which means $(P_{1/2})_{O_2}$ was lower than $(P_{1/2})_{CO}$, and the material showed adsorption selectivity close to 5 at 10 Torr in favor to dioxygen, if we consider only the chemisorption processes. The chemisorption capacity was slightly higher for CO than for O_2 (4.80 and 3.95 $cm^3 g^{-1}$ for **M1CuCl$_2$** respectively, see Table S1 in the Supporting Information) and the selectivity value approached 1 if the pressure was close to 760 Torr. This indicates that the materials have a better affinity for gas molecules able to bind according to a bidentate coordination mode like O_2, instead of a monodentate way like CO in a 1:1 Cu:CO stoichiometry. Moreover, despite the high porosity of the solids, the accessibility for CO binding was very low, as the adsorbed volume V_1 related to the highest energetic contribution represented only 3% of the active sites on the total amount of 28.1% for **M1CuCl$_2$** and 17.1% for **M2CuCl$_2$**. Thus, the major contribution to CO adsorption was poorly effective in terms of affinity. Therefore, the materials displayed a high selectivity for O_2 binding thanks to the close proximity of the copper ions.

The XRD diffraction analysis (Figure 1a) of **M1CuCl$_2$** after exposure to dioxygen shows the preservation of the short-range organization of the material, but with significant modifications. The first peak becomes slightly sharper after complexation and thus leads to a slight increase of the structuration after oxygenation. Moreover, the shift of the peak related to the siloxane layers from 23° (3.9 Å) to 21.1° (4.2 Å) corresponds to an increase of the distance between two interlamellar plans. As a consequence, it can be concluded that the organosilica wall thickness slightly increased after complexation and O_2 coordination, and demonstrates that the motion of the ligand during complexation also generates the global flexibility of the silica network. The structuration improvement observed after oxygenation and the adaptability of the TREN tripodal complexes to the trigonal-bipyramidal as well as square-pyramidal geometries required for copper cations thanks to the Berry rotation[103,104] explain the very good reversibility of the oxygenation reaction evidenced in Figure S3 in the Supporting Information. The reactivity of

M1$CuCl_2$ towards dioxygen is thus explained by the adaptability of the tripodal ligand to the different geometries required by the copper centers in relation to their redox states.

After exposure to dioxygen, **M2**$CuCl_2$ displayed a diffraction peak at 5.8°, related to the organic parts (Figure 1b), which is broader and less intense than the material before metalation and oxygenation. This can be attributable to a decrease of the short-range organization in the walls of the framework in contrast to what was observed for **M1**$CuCl_2$. In the same time, the amount of reversible chemisorbed dioxygen was lower than for **M1**$CuCl_2$ (see Table S1 in the Supporting Information). Hence, it can be concluded that metal imprinting is required to control the geometry of the tripodal copper complexes and better structuration in the short range to induce a high reactivity of the metalated materials towards dioxygen and a high reversibility of the oxygenation reaction. A straightforward structure–reactivity correlation is therefore demonstrated.

Compared to the reactivity of copper(I) tripodal complexes in solution, the dioxygen adduct is much better stabilized in the silica matrix since the copper–O_2 adduct of TREN is only stable in solution at low temperature and Cu^I cannot be regenerated when degassing.[20,21,24] However, such stability and reversibility of the dioxygen adduct at room temperature were only described recently in the solid state for an end-on μ-peroxodicopper complex with Me_6TREN[25] and in organic solution for an end-on superoxocopper complex with TREN functionalized by three tetramethylguanidine groups.[22,23,105] This confirms the original biomimetic properties of our material that incorporates tripodal complexes. In addition to the high reactivity of the materials thanks to the adaptability of the tripodal complexes to the different geometries, the stability of the dioxygen adduct can also be explained by the confinement of the active species encapsulated in the silica framework that protects them from degradation, by, for example, hydrolysis of the peroxide or ligand oxidation. The silica matrix acts as a shell and plays a similar role to that of proteins for active sites of copper metalloenzymes like haemocyanin. Therefore, the engineering of the metal-ion microenvironment and the ion confinement in the solid are prerequisites to stabilize copper–dioxygen adducts at room temperature.

Spectroscopic studies and Cu–O_2 binding mode: UV/Vis and EPR spectroscopies were used to determine the coordination scheme of the metallic cations and to gauge the ligand field stabilization energy (LFSE) of the complexes in **M1**, as well as to elucidate the structure of the copper–dioxygen adduct. As the electronic properties of the complexes are strictly dependent on the axial and equatorial donor strength, different spectral morphologies might be expected at different preparation steps and after exposure to dioxygen. Figure 3 shows UV/Vis and EPR spectra recorded at 100 K for the copper complex precursor and the metalated materials.

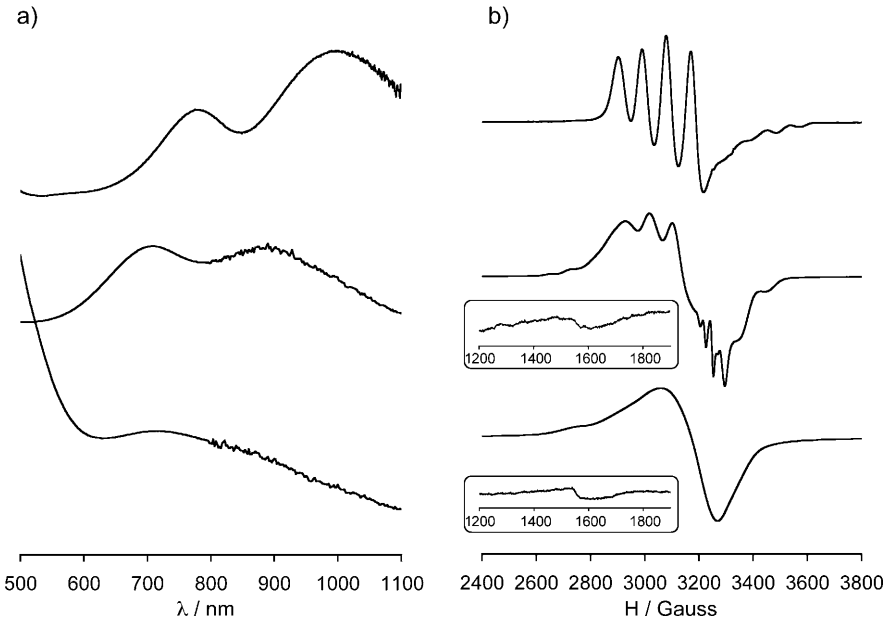

Figure 3. a) UV/Vis and b) EPR spectra for (top to bottom): [Cu(L)Br]Br precursor (in CH_2Cl_2 at 293 K for UV/vis and DMF/toluene 3/1 at 100 K for EPR), **M1** before de-metalation and surfactant extraction, and **M1**$CuCl_2$ after exposure to O_2. Inserts in b) represent the half-field transitions in the EPR spectra.

Owing to the tripodal arrangement of the four nitrogen donor atoms, TREN ligands are ideal candidates to prepare metal complexes possessing a trigonal-bipyramidal geometry, and a variety of copper(II) coordination compounds with this geometry have been reported[106] both in the solid state and in solution.[107,108] The electronic transition of lowest energy was assigned to the promotion of one electron from the degenerate d_{xy}, $d_{x^2-y^2}$ orbitals to the d_{z^2} orbital and the less intense band to the d_{xz}, $d_{yz} \rightarrow d_{z^2}$ transition, both being allowed in a C_{3v} symmetry.[109–111] For the silylated precursor [Cu(**L**)Br]Br in dichloromethane (Figure 3 and Table S3 in the Supporting Information) before incorporation in the material, the UV/Vis data are consistent with a trigonal-bipyramidal geometry since a maximum at $\lambda =$ 993 nm ($\varepsilon = 165$ mol^{-1} dm^3 cm^{-1}) and a less intense band at $\lambda = 776$ nm ($\varepsilon = 125$ mol^{-1} dm^3 cm^{-1}) were observed.[109,111] These data are similar to those displayed by [Cu(Me_6TREN)Br]Br, thus indicating a negligible effect of the alkyl chain length on the LFSE.[111]

The EPR spectrum of [Cu(**L**)Br]Br in frozen dimethylformamide–toluene (3:1 v/v) gave g and A factors comparable with those of other TREN-type complexes known to display trigonal-bipyramidal geometry.[108–111] The spectrum exhibited a magnetic anisotropy with parallel and perpendicular components typical for a doublet spin state. The hyperfine coupling between the unpaired electron and the copper(II) nucleus ($I=3/2$) produces four lines with $A_{\perp}=93\times10^{-4}\,cm^{-1}$ and $A_{\parallel}=75\times10^{-4}\,cm^{-1}$ (see Table S3 in the Supporting Information). The sequence $g_{\perp}=2.18>g_{\parallel}=1.92$ was also indicative of a trigonal-bipyramidal geometry with a magnetic orbital in the ground state corresponding to d_{z^2}. The $g_{\parallel}$value lies slightly above the free electron value (2.0023) that suggests a significant mixing between d_{xz}, d_{yz} orbitals and the d_{z^2} ground state, which occurs by vibronic coupling and thanks to the large spin-orbit coupling of the halide lying in apical position.[110]

After formation of **M1**, but before extraction of the surfactant (Figure 3a, middle curves), the UV/Vis spectrum exhibited two absorption bands with the same intensities and a blue shift compared to [Cu(**L**)Br]Br. This indicates that the immobilized complexes possess an intermediate geometry between a trigonal-bipyramidal and a square-based pyramidal geometry. Analysis of the EPR spectrum (Figure 3b, middle curves) clearly indicates this intermediate geometry; it can be considered as the overlap of spectra corresponding to these two coordination schemes. A dinuclear complex was also formed, as revealed by the presence of a weak forbidden transition at half field characteristic of a dipolar coupling between two adjacent copper ions in the silica framework, leading to a triplet spin state with a weak zero-field splitting.

After re-metalation and oxygenation (Figure 3a, bottom curve), the UV/Vis spectrum exhibited a large absorption band centered at $\lambda=720$ nm and a shoulder around $\lambda=900$ nm, indicative of a square-based pyramidal complex, as already described for copper tetraazamacrocycle complexes immobilized in a sol–gel matrix,[35] in which the axial nitrogen atom of the bipyramidal structure became equatorial in the tetragonal pyramid. This stereochemistry is thus consistent with a C_{4v} symmetry and a $d_{x^2-y^2}$ ground state.[112] The weak energy transition compared to other CuN_5X complexes[113] indicates also a slight distortion in the equatorial plane. Hence, there is a significant evolution of the copper coordination polyhedra during the formation of **M1** after re-metalation and oxygenation. These phenomena can be explained by steric constraints applied to the ligands by the silica framework. It is well known that distortions in the equatorial plane can occur if the steric hindrance on the terminal nitrogen donors or axial ligand field increases. As shown by X-ray crystallography,[24] and UV/Vis and EPR spectroscopies,[111] the introduction of bulky substituents on the nitrogen atoms of the TREN skeleton weakens the ligand-field strength and, in extreme cases,[114] the expected trigonal-bipyramidal stereochemistry switch to a square-pyramidal geometry of copper ions thanks to the Berry rotation.[103,104,107] Therefore, intermediate geometries have been often obtained.[115] The dynamic effect in the material was attributed to the flexibility of the *N*-alkyl chains and to the topological adaptability of the TREN complexes to both coordination schemes.[103,104,107] This stereochemical evolution illustrates the flexibility of the material as previously shown by using XRD measurements.

Examination of the EPR spectrum of **M1 CuCl$_2$** after oxygenation (Figure 3b, bottom curve) showed a spectrum with an axial g tensor at $g_{\parallel}\approx 2.26$ ($A_{\parallel}\approx180\times10^{-4}\,cm^{-1}$) and $g_{\perp}\approx2.09$ characteristic of a Cu^{II} ion in a tetragonal environment with a small distorted C_{4v} symmetry and a nearly axial g tensor.[109,116] The fact that $g_{\parallel}>g_{\perp}>2.0023$ is also indicative of a $d_{x^2-y^2}$ magnetic orbital as expected for this coordination geometry. The low resolution of the hyperfine structure observed in the EPR spectra before de-metalation and after re-metalation indicated spin–spin interactions between copper(II) ions, which were assigned to the high concentration of copper(II) in the material. The broad linewidth in the range 2500 to 3600 G ($\Delta M_s=1$) is thus typical of dipolar interactions between metal ions. A half-field forbidden transition ($\Delta M_s=2$) was also observed at half field (1550 G).[117,118] This signal is attributed to a triplet spin state with a weak zero-field splitting, which means two copper(II) ions are weakly coupled. No strong magnetic exchange interaction between two $[Cu(TREN)]^{2+}$ moieties exists otherwise a narrowing of the lines would be observed.

These results are in contradiction with the assumed active sites, which are supposed to be dicopper complexes in close interaction that form μ-peroxo dioxygen species. Indeed, as reported for copper metalloproteins and model complexes,[3,19] the antiferromagnetically coupling between the two unpaired electrons in a bridged peroxodicopper complex leads to an EPR-silent singlet ground state. Moreover, the intermediate superoxide is also diamagnetic, owing to the strong coupling between the unpaired electron of the superoxide and that of Cu^{II}.[119] Hence, whatever dioxygen adduct formed, no EPR signal should be observed, which contrasts with the O_2 species in the materials described herein.

Elucidation of the copper–dioxygen adduct and the active complexes before oxygenation will provide a better understanding of the exceptional reactivity of the materials towards dioxygen and the stability of the O_2 adduct. Additional information was obtained by completing quantitative EPR measurements and UV/Vis monitoring during exposure to dioxygen.

The concentration of EPR-active copper(II) in **M1 CuCl$_2$** after activation at 393 K (see Figure S4 in the Supporting Information) was analyzed by quantitative EPR measurements by using silica diluted copper standards of known concentration. The intensity of the EPR spectrum increased regularly during exposure to O_2 at 293 K, which revealed that the dioxygen species formed are paramagnetic and that the antiferromagnetic coupling between two adjacent copper atoms was weak. After 25 h, the percentage of EPR-active copper had reached 40% of the total metal amount. Since the adsorption measurements showed that only 23% of the copper

ion was active towards O_2 binding, the discrepancy between these two values led us to assume a 2:1 Cu:O_2 stoichiometry, which means that the main O_2 species formed is a dinuclear peroxo complex. Notably, the observed EPR signal cannot result from the degradation of the dioxygen adduct since we have pointed out the full reversibility of the O_2 binding for **M1 CuCl$_2$**. These measurements also show that before oxygenation the copper oxidation state was mainly +I in the material and 89% of the copper was EPR-inactive at this stage. Since a copper(II) salt ($CuCl_2$) was used as the complexing agent, a reduction of Cu^{II} to Cu^{I} has occurred during the activation step. Ethanol, the solvent used for the metalation reaction, was suspected to be the reducing agent, as previously observed with xerogels incorporating tetraazamacrocycles.[35] Hence, this redox process seems to occur whatever the polyamine immobilized in the silica matrix and whatever the synthetic method used. These redox properties can be compared to those known for copper-exchange zeolites.[120–124] Actually, a radical self-reduction mechanism has been established for Cu-ZSM-5 or Cu-MFI upon thermal treatment under vacuum.

Moreover, lower reactivity towards dioxygen was noted when **M1** is metalated with copper(II) chloride (less than 0.5 equivalent). This result demonstrates that two copper atoms in close proximity are required for O_2 coordination and that the formation of the O_2 dinuclear complex is the driving force of the oxygenation process and not the formation of the mononuclear superoxide. The nature of the metal-bound chelate, as well as the oxygenated species, is critically dependent on the nature of the multidentate ligands, which dictates the coordination geometry of the complexes, their structure, and their reactivity.[125] Much research in biomimetic chemistry has shown that the structure and reactivity of Cu–O_2 adducts are dictated by ligand denticity and electronic properties.[12,13,125,126] Generally, copper(I) complexes with tetradentate nitrogen-based ligands, such as TREN or TMPA (tris(methylpyridine)amine), prefer to form μ-1,2-peroxodicopper(II) complexes in an end-on coordination mode.[19,24] Considering this point, the copper–dioxygen adduct formed is most probably a dinuclear μ-η^1:η^1-peroxo complex.

After exposure to O_2, the significant increase of the EPR signal intensity strongly supports the formation of an unusual dioxygen adduct, which could be explained by the formation of a distorted μ-peroxide species leading to a low overlap of the magnetic orbitals. For the oxyhemocyanin copper–metalloenzyme, as well as for biomimetic complexes, such as tripodal $[Cu(TREN)]^{2+}$, it is well known that the unpaired electron is localized in the d_{z^2} orbital of copper(II),[109–111] which explains the strong antiferromagnetic coupling between the metallic ions through the bridging peroxo in an axial position. Therefore, a strong antiferromagnetic coupling occurs and the μ-peroxodicopper(II) complexes are EPR-silent. In addition, for the TREN-immobilizing materials, we have shown that the unpaired electron is localized in the copper $d_{x^2-y^2}$ orbital, which does not favor a strong coupling between metal ions through the axial peroxo bridge. Hence, it can be concluded that the singular paramagnetic properties of the μ-η^1:η^1-peroxo dimer in the material result from the unusual $d_{x^2-y^2}$ ground state of the copper(II)–TREN immobilized complexes.

The μ-η^1:η^1-peroxodicopper(II) species is formed after the **M1** copper complexes are arranged in a face-to-face manner, to allow further coordination of dioxygen between two copper ions. Moreover, the presence of metal–metal interactions in the material before extraction of the surfactant, and for **M1 CuCl$_2$** after oxygenation, indicates the formation of a μ-halide or a μ-hydroxo bridge linking two vicinal copper ions.[127]

To study the halide effect on the oxygenation process, **M1** was metalated with copper(II) bromide to yield **M1 CuBr$_2$**. After activation by heating under vacuum, significantly less reactivity (≈half) towards dioxygen was observed compared to the **M1 CuCl$_2$** analogue. This means that chloride counteranions play a key role for O_2 coordination on the copper ions and this result is consistent with a μ-chloro dinuclear complex in the case of **M1 CuCl$_2$** (Scheme 2).

Oxygenation studies of **M1 CuCl$_2$** were followed by diffuse reflectance kinetics in the visible region, and Figure 4 shows the evolution of the spectra during oxygenation of the material. The more intense band at $\lambda = 320$ nm, corresponding to LMCT, was assigned to $\sigma_N \rightarrow d_{Cu}$ and O_2^{2-} $(\pi^*_\sigma) \rightarrow d_{Cu}$ transitions, and the band at $\lambda = 450$ nm to Cl→Cu charge transfer. The copper d–d transitions displayed a broad absorption centered at $\lambda = 700$ nm. During the oxygenation, the two bands at $\lambda = 320$ and 700 nm rose continuously, whereas the band at $\lambda = 450$ nm reached a maximum and decreased in a second step. Finally, the absence of a d–d transition before exposure to dioxygen clearly indicates that copper was mainly in the +I oxidation state in the material, as shown previously by EPR spectroscopy. The increase of the d–d transition at $\lambda = 700$ nm reflects the oxidation to copper(II) and the evolution of the band at $\lambda = 450$ nm indicates that chloride ions play a major role in the oxygenation process. Therefore, these data confirm the formation of a species in which a bridging chloride occurs in the dinuclear μ-η^1:η^1-peroxide copper complex (Scheme 2). Notably, the electronic

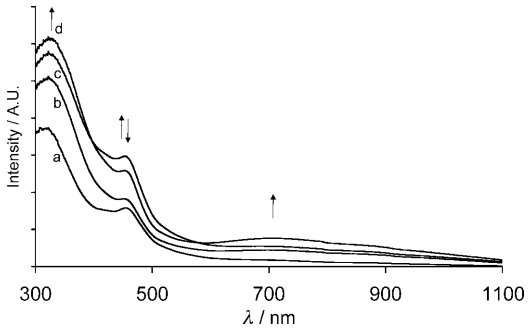

Figure 4. Solid-state diffuse reflectance spectra evolution in the visible region for **M1 CuCl$_2$** during exposure to dioxygen for a) 2 min, b) 4 min, c) 20 min, and d) 24 h.

data for the dioxygen adduct is quite different to that for the known μ-η^1:η^1-peroxodicopper(II) or end-on superoxide, which demonstrates the unusual O_2 species formed.[12,24,105,128]

The exceptional reactivity of the described materials is a consequence of the short-range order of the copper complexes in the silica framework occurring during the hydrolytic polycondensation of the alkoxysilylated TREN precursor. Hence, the reactivity is in agreement with an anisotropic distribution of the ligand in a lamellar structure, and the active complexes display a packing of the tripodal complexes in close proximity allowing formation of dimeric O_2 adducts. As already observed for silylated aryl or alkyl chains,[59,75,87–96] hydrolytic polycondensation of organosilylated spacers often leads to nanostructured solids, at least at the molecular scale, thanks to van der Waals interactions or hydrogen bonds occurring between the hydrophobic or the hydrophilic (silanols) parts of the hydrolyzed organic precursors. It was thus shown that even molecular precursors with flexible alkyl chains can lead to nano-organization of the materials over short or long ranges.[89,90,92,94,96,129] As shown previously, analysis of XRD data has indicated that the flexible structure of the peripheral *N*-alkyl chains of the ligand leads to a global flexibility and to a breathing hybrid material. Such behavior provides a fine-tuning of the metal–metal distance suitable for the formation of dinuclear O_2 adducts.

The immobilization of TREN derivatives in the framework of a silica matrix allows unusual metal coordination properties, stereochemistry, and oxidation states of copper that cannot be observed in solution. Moreover, the copper–dioxygen adducts are stable at room temperature thanks to the confinement of the encapsulated active species in the hybrid framework that fully protects the dioxygen species from degradation. This illustrates the original biomimetic properties of these materials. Therefore, the control of the metal-ion environment and their confinement in the solid are required to stabilize the copper–dioxygen adducts at room temperature.

Conclusion

We have prepared by a double-printing method in basic medium porous organosilica incorporating a TREN derivative, which were able, after complexation by copper(II) chloride and thermal activation, to coordinate reversibly molecular oxygen at room temperature. The copper–dioxygen species formed was postulated to be an end-on μ-η^1:η^1-peroxo dinuclear complex bridged by a chloride counterion. The copper–O_2 adducts did not decompose at room temperature since several oxygenation/deoxygenation cycles were possible with 97% reversibility after four cycles. The high reactivity and reversibility of the materials for dioxygen binding were explained by the topological adaptability of the tripodal ligand to different geometries required by the copper ion in different oxidation states. Moreover, the metal ion imprinting effect was clearly shown to control the topology and the coordination properties of the immobilized TREN. This result, which cannot be reproduced in solution, was caused by a short-range organization of the active sites in the silica framework, the flexibility of the immobilized polyamines, and the ability of the silica matrix to shield the copper complexes. As for metalloenzymes, the hydrolytic polycondensation of the active complexes creates hydrophobic cavities, which avoids any further side reactions and protects the copper–dioxygen adduct from moisture, allowing reversible binding on the metal. Such bioinspired materials behave like dioxygen carrier models of copper metalloenzymes such as haemocyanin. This conceptual approach led us to develop organic–inorganic hybrid systems with unexpected properties. Additionally, correlations between the coordination chemistry, the confinement effect of the active sites, and the reactivity towards dioxygen were clearly evident.

Experimental Section

Materials: All reagents and solvents were purchased from Acros and used without further purification. The 3-iodopropyltriethoxysilane was prepared, as previously described.[32] Ethanol, used for copper complexation of the material, and acetonitrile were distilled under argon and stored on 4 Å molecular sieves. Pentane was distilled under argon over CaH_2. Before complexation, **M1** and **M2** were dried in vacuo (10^{-3} Torr) at 393 K. Complexation of **M1** and **M2** was carried out in a glove box under an argon atmosphere. Tripodal precursors **1** and **2** were synthesized following a modification of a published procedure (see the Supporting Information).[76] Alkoxysilylated precursor **L** and its copper complex [Cu(**L**)Br]Br were prepared by using standard Schlenk techniques and dried solvent (see the Supporting Information). They can be stored for months at 5°C under argon atmosphere.

Material preparation

Framework M1: CTAB (0.839 g) and NaOH (0.276 g) were dissolved in deionized water (45 mL) and stirred for 10 min. A solution containing [Cu(**L**)Br]Br (1.26 g) and TEOS (2.46 g) was then added and stirred at room temperature for 1 h followed by 80°C for 3 days to ensure polycondensation. The solid obtained was filtered and rinsed with water and EtOH. The surfactant was extracted by refluxing for five hours in acidified ethanol (1 M) with concentrated hydrochloric acid. After filtration and rinsing with EtOH, the incorporated amine was deprotonated by stirring the material in EtOH (100 mL) containing a twofold excess of triethylamine (1.32 mL) for 20 min. Filtration of the solid and rinsing with EtOH yielded **M1** as a white powder (1.08 g, 83%). The synthesis was done according to a Si/CTAB/NaOH/H_2O molar ratio of 1:0.15:0.45:160. $S_{BET}=489\ m^2 g^{-1}$; $D_p<30$ Å; $V_p=0.29\ cm^3 g^{-1}$; ^{29}Si NMR (99 MHz, CP/MAS): $\delta=-57.6$ (T^2), -64.1 (T^3), -90.9 (Q^2), -99.3 (Q^3), -107.9 ppm (Q^4); ^{13}C NMR (125 MHz, CP/MAS): $\delta=55.4$, 51.7, 21.7, 12.7 ppm; IR (ATR): $\tilde{\nu}=2968$ (ν_{as}(C–H)), 2877 (ν_s(C–H)), 1469 (δ(C–H)), 1200–1000 (ν_{as}(Si-O-Si)), 958 (ν_{as}(Si–OH)), 816 cm^{-1} (δ(Si-OH)); elemental analysis calcd (%) for $C_{21}H_{45}N_4O_{24.5}Si_{13}\cdot 1.5\,H_2O\cdot 0.25$ CTAC (1218.61): C 25.43, H 4.85, N 4.89, Si 29.96; found: C 25.37, H 5.07, N 5.34, Si 27.82, which gives a ligand concentration of 0.82 mmol g^{-1}.

Framework M2: The procedure described for **M1** was used to prepare **M2** starting from **L** instead of [Cu(**L**)Br]Br, to yield **M2** as a white powder (83%). $S_{BET}=210\ m^2 g^{-1}$; $D_p<30$ Å; $V_p=0.13\ cm^3 g^{-1}$; elemental analysis calcd (%) for $C_{21}H_{45}N_4O_{24.5}Si_{13}\cdot 0.3$ CTAC (1206.71): C 26.58, H 4.81, N 4.99; found: C 26.48, H 5.12, N 5.62, which gives a ligand concentration of 0.83 mmol g^{-1}.

Material complexation

Framework M1 $CuCl_2$: In a glove box, **M1** (0.40 g) was suspended in thoroughly dried and degassed EtOH (7 mL), and an ethanolic solution of

anhydrous $CuCl_2$ (0.056 g, 20% excess) was added under stirring. After the mixture had been refluxed for 3 h, the solid was filtered and washed with EtOH (2×10 mL). The drying and activation of the material was done by heating in vacuo (10^{-3} Torr) for 5 h at 393 K to give **M1 CuCl$_2$** as a clear brown solid (0.43 g, 97%). $S_{BET}=296\ m^2g^{-1}$; $D_p<30$ Å; $V_p=0.17\ cm^3g^{-1}$; elemental analysis calcd (%) for $C_{21}H_{45}N_4O_{24,5}Si_{13}CuCl_2{\cdot}4H_2O{\cdot}0.1$ CTAC (1349.22): C 20.39, H 4.27, N 4.26, Si 27.06, Cu 4.71; found: C 20.25, H 4.00, N 4.30, Si 26.97, Cu 4.85, which gives a ligand concentration of 0.74 mmol g^{-1} and a metal concentration of 0.76 mmol g^{-1}.

Framework M2 CuCl$_2$: This compound was prepared following the procedure described for **M1 CuCl$_2$** starting from **M2** (0.40 g) instead of **M1**, to yield **M2 CuCl$_2$** as a clear brown solid (0.44 g, 99%). $S_{BET}=161\ m^2g^{-1}$; $D_p<30$ Å; $V_p=0.10\ cm^3g^{-1}$; elemental analysis calcd (%) for $C_{21}H_{45}N_4O_{24,5}Si_{13}CuCl_2{\cdot}14H_2O$ (1497.37): C 16.84, H 4.91, N 3.74, Si 24.38, Cu 4.24; found: C 16.70, H 4.74, N 3.75, Si 22.46, Cu 5.15, which gives a ligand concentration of 0.67 mmol g^{-1} and a metal concentration of 0.81 mmol g^{-1}.

Framework M1 CuBr$_2$: This compound was prepared following the procedure described for **M1 CuCl$_2$** starting from **M1** (0.40 g) and anhydrous $CuBr_2$ (0.088 g, 20% excess), to yield **M1 CuBr$_2$** as a clear brown solid (0.43 g, 93%). $S_{BET}=79\ m^2g^{-1}$; $D_p<30$ Å; $V_p=0.10\ cm^3g^{-1}$; UV/Vis (diffuse reflectance): $\lambda=710$, 890 nm; elemental analysis calcd (%) for $C_{21}H_{45}N_4O_{24,5}Si_{13}CuBr_2{\cdot}12H_2O{\cdot}0.15$ CTAC (1598.25): C 17.92, H 4.75, N 3.64, Si 22.84, Cu 3.98; found: C 17.78, H 4.74, N 4.15, Si 21.49, Cu 3.75, which gives a ligand concentration of 0.63 mmol g^{-1} and a metal concentration of 0.59 mmol g^{-1}.

Characterization: Materials were characterized at the "Plateforme d'Analyse Chimique et de Synthèse Moléculaire de l'Université de Bourgogne (PACSMUB)" by using a FTIR spectrometer equipped with a BRUKER Golden Gate Vector 22 in ATR mode and a solid-state UV/Vis spectrometer recording in the diffuse reflectance mode by using a VARIAN Cary 500. Continuous wave (CW) EPR spectra were recorded by using a BRUKER ELEXSYS 500 spectrometer available at the "PACSMUB" equipped with a 4122 SHQE/0405 X-band resonant cavity operating at 9.43 GHz and a quartz cryostat cooled with a stream of nitrogen. Powder X-ray diffraction experiments were carried out by using a INEL diffractometer with a curved counter CPS 120 using the $Cu_{K\alpha}$ radiation between 2° and 100° (2 theta). The organic content of all samples was determined from CHN elemental analyses performed by using a FTA/Thermofinnigan Flash 1112 analyser while Cu and Si microanalyses were obtained from the "Service Central d'Analyse du CNRS, Lyon". Specific surface areas were measured by N_2 adsorption measurements performed at 77 K using the Brunauer–Emmet–Teller method[130] (BET) on a MICROMERITICS ASAP 2010 analyser in the relative P/P_0 pressure range from 0.05 to 0.25. The cross-sectional area of the nitrogen molecule was assumed to be equal to 0.162 nm^2. Average pore diameters were calculated using the Barrett–Joyner–Halenda analysis (BJH).[86] Each sample was previously degassed by heating at 393 K in vacuo (10^{-3} Torr) for at least 3 h. The equilibrium constants for the gas binding affinity, K_i, and the adsorption capacity, V_i, were calculated by considering a dual site adsorption model (see the Supporting Information).[32,33,35]

Acknowledgements

This work was supported by the CNRS. C.S. gratefully acknowledges the Région Bourgogne for a financial support.

[1] J. P. Klinman, *Chem. Rev.* **1996**, *96*, 2541–2562.
[2] E. I. Solomon, U. M. Sundaram, T. E. Machonkin, *Chem. Rev.* **1996**, *96*, 2563–2605.
[3] E. I. Solomon, P. Chen, M. Metz, S.-K. Lee, A. E. Palmer, *Angew. Chem.* **2001**, *113*, 4702–4724; *Angew. Chem. Int. Ed.* **2001**, *40*, 4570–4590.
[4] E. I. Solomon, R. Sarangi, J. S. Woertink, A. J. Augustine, J. Yoon, S. Ghosh, *Acc. Chem. Res.* **2007**, *40*, 581–591.
[5] E. I. Solomon, A. J. Augustine, J. Yoon, *Dalton Trans.* **2008**, 3921–3932.
[6] I. A. Koval, P. Gamez, C. Belle, K. Selmeczi, J. Reedijk, *Chem. Soc. Rev.* **2006**, *35*, 814–840.
[7] S. Schindler, *Eur. J. Inorg. Chem.* **2000**, 2311–2326.
[8] S. T. Prigge, B. A. Eipper, R. E. Mains, L. M. Amzel, *Science* **2004**, *304*, 864–867.
[9] K. A. Magnus, H. Tonthat, J. E. Carpenter, *Chem. Rev.* **1994**, *94*, 727–735.
[10] M. Metz, E. I. Solomon, *J. Am. Chem. Soc.* **2001**, *123*, 4938–4950.
[11] E. I. Solomon, M. J. Baldwin, M. D. Lowery, *Chem. Rev.* **1992**, *92*, 521–542.
[12] L. M. Mirica, X. Ottenwaelder, T. D. P. Stack, *Chem. Rev.* **2004**, *104*, 1013–1045.
[13] E. A. Lewis, W. B. Tolman, *Chem. Rev.* **2004**, *104*, 1047–1076.
[14] L. M. Mirica, D. J. Rudd, M. A. Vance, E. I. Solomon, K. O. Hodgson, B. Hedman, T. D. P. Stack, *J. Am. Chem. Soc.* **2006**, *128*, 2654–2665.
[15] M. Suzuki, *Acc. Chem. Res.* **2007**, *40*, 609–617.
[16] C. J. Cramer, W. B. Tolman, *Acc. Chem. Res.* **2007**, *40*, 601–608.
[17] T. Matsumoto, K. Ohkubo, K. Honda, A. Yazawa, H. Furutachi, S. Fujinami, S. Fukuzumi, M. Suzuki, *J. Am. Chem. Soc.* **2009**, *131*, 9258–9267.
[18] R. R. Jacobson, Z. Tyeklar, A. Farooq, K. D. Karlin, S. Liu, J. Zubieta, *J. Am. Chem. Soc.* **1988**, *110*, 3690–3692.
[19] Z. Tyeklar, R. R. Jacobson, N. Wei, N. N. Murthy, J. Zubieta, K. D. Karlin, *J. Am. Chem. Soc.* **1993**, *115*, 2677–2689.
[20] K. D. Karlin, N. Wei, B. Jung, S. Kaderli, P. Niklaus, A. D. Zuberbühler, *J. Am. Chem. Soc.* **1993**, *115*, 9506–9514.
[21] M. Weitzer, S. Schindler, G. Brehm, S. Schneider, E. Hörmann, B. Jung, S. Kaderli, A. D. Zuberbühler, *Inorg. Chem.* **2003**, *42*, 1800–1806.
[22] M. Schatz, V. Raab, S. P. Foxon, G. Brehm, S. Schneider, M. Reiher, M. C. Holthausen, J. Sundermeyer, S. Schindler, *Angew. Chem.* **2004**, *116*, 4460–4464; *Angew. Chem. Int. Ed.* **2004**, *43*, 4360–4363.
[23] C. Würtele, E. Gaoutchenova, K. Harms, M. C. Holthausen, J. Sundermeyer, S. Schindler, *Angew. Chem.* **2006**, *118*, 3951–3954; *Angew. Chem. Int. Ed.* **2006**, *45*, 3867–3869.
[24] K. Komiyama, H. Furutachi, S. Nagatomo, A. Hashimoto, H. Hayashi, S. Fujinami, M. Suzuki, T. Kitagawa, *Bull. Chem. Soc. Jpn.* **2004**, *77*, 59–72.
[25] C. Würtele, O. Sander, V. Lutz, T. Waitz, F. Tuczek, S. Schindler, *J. Am. Chem. Soc.* **2009**, *131*, 7544–7545.
[26] J. E. Bol, W. L. Driessen, R. Y. N. Ho, B. Maase, L. Que, J. Reedijk, *Angew. Chem.* **1997**, *109*, 1022–1025; *Angew. Chem. Int. Ed. Engl.* **1997**, *36*, 998–1000.
[27] M. Kodera, K. Katayama, Y. Tachi, K. Kano, S. Hirota, S. Fujinami, M. Suzuki, *J. Am. Chem. Soc.* **1999**, *121*, 11006–11007.
[28] H. Börzel, P. Comba, K. S. Hagen, M. Kerscher, H. Pritzkow, M. Schatz, S. Schindler, O. Walter, *Inorg. Chem.* **2002**, *41*, 5440–5452.
[29] M. Kodera, Y. Kajita, Y. Tachi, K. Katayama, K. Kano, S. Hirota, S. Fujinami, M. Suzuki, *Angew. Chem.* **2004**, *116*, 338–341; *Angew. Chem. Int. Ed.* **2004**, *43*, 334–337.
[30] L. Q. Hatcher, M. A. Vance, A. A. N. Sarjeant, E. I. Solomon, K. D. Karlin, *Inorg. Chem.* **2006**, *45*, 3004–3013.
[31] D. Maiti, A. A. Narducci Sarjeant, K. D. Karlin, *J. Am. Chem. Soc.* **2007**, *129*, 6720–6721.
[32] G. Dubois, R. Tripier, S. Brandès, F. Denat, R. Guilard, *J. Mater. Chem.* **2002**, *12*, 2255–2261.
[33] J.-M. Barbe, G. Canard, S. Brandès, F. Jerome, G. Dubois, R. Guilard, *Dalton Trans.* **2004**, 1208–1214.
[34] J. M. Barbe, G. Canard, S. Brandès, R. Guilard, *Chem. Eur. J.* **2007**, *13*, 2118–2129.
[35] S. Brandès, G. David, C. Suspène, R. J. P. Corriu, R. Guilard, *Chem. Eur. J.* **2007**, *13*, 3480–3490.

[36] R. M. Izatt, K. Pawlak, J. S. Bradshaw, R. L. Bruening, *Chem. Rev.* **1995**, *95*, 2529–2586.
[37] M. Meyer, V. Dahaoui-Gindrey, C. Lecomte, R. Guilard, *Coord. Chem. Rev.* **1998**, *178–180*, 1313–1405.
[38] C. Gros, F. Rabiet, F. Denat, S. Brandès, H. Chollet, R. Guilard, *J. Chem. Soc. Dalton Trans.* **1996**, 1209–1214.
[39] R. J. P. Corriu, A. Mehdi, C. Reye, C. Thieuleux, *Chem. Mater.* **2004**, *16*, 159–166.
[40] F. Cuenot, M. Meyer, A. Bucaille, R. Guilard, *J. Mol. Liq.* **2005**, *118*, 89–99.
[41] M. Etienne, S. Goubert-Renaudin, Y. Rousselin, C. Marichal, F. Denat, B. Lebeau, A. Walcarius, *Langmuir* **2009**, *25*, 3137–3145.
[42] S. Goubert-Renaudin, M. Etienne, S. Brandès, M. Meyer, F. Denat, B. Lebeau, A. Walcarius, *Langmuir* **2009**, *25*, 9804–9813.
[43] R. J. P. Corriu, A. Mehdi, C. Reyé, C. Thieuleux, *Chem. Commun.* **2002**, 1382–1383.
[44] R. J. P. Corriu, A. Mehdi, C. Reyé, C. Thieuleux, *Chem. Commun.* **2003**, 1564–1565.
[45] R. J. P. Corriu, A. Mehdi, C. Reyé, C. Thieuleux, *New J. Chem.* **2003**, *27*, 905–908.
[46] J. Goulon, C. Goulon-Ginet, A. Rogalev, F. Wilhelm, N. Jaouen, D. Cabaret, Y. Joly, G. Dubois, R. J. P. Corriu, G. David, S. Brandès, R. Guilard, *Eur. J. Inorg. Chem.* **2005**, 2714–2726.
[47] R. J. Motekaitis, A. E. Martell, J. M. Lehn, E. Watanabe, *Inorg. Chem.* **1982**, *21*, 4253–4257.
[48] T. Asefa, C. Yoshina-Ishii, M. J. MacLachlan, G. A. Ozin, *J. Mater. Chem.* **2000**, *10*, 1751–1755.
[49] G. Kickelbick, *Angew. Chem.* **2004**, *116*, 3164–3166; *Angew. Chem. Int. Ed.* **2004**, *43*, 3102–3104.
[50] M. P. Kapoor, S. Inagaki, *Bull. Chem. Soc. Jpn.* **2006**, *79*, 1463–1475.
[51] Q. Yang, J. Liu, C. Li, *J. Mater. Chem.* **2009**, *19*, 1945–1955.
[52] S. Inagaki, S. Guan, Y. Fukushima, T. Ohsuna, O. Terasaki, *J. Am. Chem. Soc.* **1999**, *121*, 9611–9614.
[53] B. J. Melde, B. T. Holland, C. F. Blanford, A. Stein, *Chem. Mater.* **1999**, *11*, 3302–3308.
[54] T. Asefa, M. J. MacLachlan, N. Coombs, G. A. Ozin, *Nature* **1999**, *402*, 867–871.
[55] F. Hoffmann, M. Cornelius, J. Morell, M. Fröba, *Angew. Chem.* **2006**, *118*, 3290–3328; *Angew. Chem. Int. Ed.* **2006**, *45*, 3216–3251.
[56] S. Inagaki, S. Guan, T. Ohsuna, O. Terasaki, *Nature* **2002**, *416*, 304–307.
[57] W. J. Hunks, G. A. Ozin, *Chem. Mater.* **2004**, *16*, 5465–5472.
[58] M. P. Kapoor, Q. Yang, S. Inagaki, *J. Am. Chem. Soc.* **2002**, *124*, 15176–15177.
[59] K. Okamoto, M. P. Kapoor, S. Inagaki, *Chem. Commun.* **2005**, 1423–1425.
[60] Y. Liang, M. Hanzlik, R. Anwander, *J. Mater. Chem.* **2005**, *15*, 3919–3928.
[61] K. Z. Hossain, L. Mercier, *Adv. Mater.* **2002**, *14*, 1053–1056.
[62] H. Zhu, D. J. Jones, J. Zajac, R. Dutartre, M. Rhomari, J. Rozière, *Chem. Mater.* **2002**, *14*, 4886–4894.
[63] M. Álvaro, M. Benitez, D. Das, B. Ferrer, H. Garcia, *Chem. Mater.* **2004**, *16*, 2222–2228.
[64] M. Benitez, G. Bringmann, M. Dreyer, H. Garcia, H. Ihmels, M. Waidelich, K. Wissel, *J. Org. Chem.* **2005**, *70*, 2315–2321.
[65] S. Jayasundera, M. C. Burleigh, M. Zeinali, M. S. Spector, J. B. Miller, W. Yan, S. Dai, M. A. Markowitz, *J. Phys. Chem. B* **2005**, *109*, 9198–9201.
[66] J. Alauzun, A. Mehdi, C. Reyé, R. J. P. Corriu, *J. Mater. Chem.* **2007**, *17*, 349–356.
[67] C. Liu, J. B. Lambert, L. Fu, *J. Am. Chem. Soc.* **2003**, *125*, 6452–6461.
[68] M. A. Karakassides, A. Bourlinos, D. Petridis, L. Coche-Guerente, P. Labbè, *J. Mater. Chem.* **2000**, *10*, 403–408.
[69] C.-H. Lee, H.-C. Lin, S.-H. Cheng, T.-S. Lin, C.-Y. Mou, *J. Phys. Chem. C* **2009**, *113*, 16058–16069.
[70] R. D. Makote, S. Dai, *Anal. Chim. Acta* **2001**, *435*, 169–175.
[71] D. Rechavi, B. Albela, L. Bonneviot, M. Lemaire, *Tetrahedron* **2005**, *61*, 6976–6981.
[72] J. L. Defreese, A. Katz, *Chem. Mater.* **2005**, *17*, 6503–6506.
[73] S. Abry, A. Thibon, B. Albela, P. Delichère, F. Banse, L. Bonneviot, *New J. Chem.* **2009**, *33*, 484–496.
[74] B. Boury, R. J. P. Corriu, *Chem. Commun.* **2002**, 795–802.
[75] B. Boury, R. J. P. Corriu, *Chem. Rec.* **2003**, *3*, 120–132.
[76] K. E. Krakowiak, J. S. Bradshaw, R. M. Izatt, *J. Org. Chem.* **2002**, *67*, 3364–3368.
[77] M. C. Burleigh, S. Dai, E. W. Hagaman, J. S. Lin, *Chem. Mater.* **2001**, *13*, 2537–2546.
[78] Y.-K. Lu, X.-P. Yan, *Anal. Chem.* **2004**, *76*, 453–457.
[79] E. Besson, A. Mehdi, C. Reyé, R. J. P. Corriu, *J. Mater. Chem.* **2006**, *16*, 246–248.
[80] W. Guo, X. Li, X. S. Zhao, *Microporous Mesoporous Mater.* **2006**, *93*, 285–293.
[81] Y. Wan, D. Zhao, *Chem. Rev.* **2007**, *107*, 2821–2860.
[82] D. Zhao, Q. Huo, J. Feng, B. F. Chmelka, G. D. Stucky, *J. Am. Chem. Soc.* **1998**, *120*, 6024–6036.
[83] G. J. A. A. Soler-Illia, C. Sanchez, B. Lebeau, J. Patarin, *Chem. Rev.* **2002**, *102*, 4093–4138.
[84] K. S. W. Sing, D. H. Everett, R. A. W. Haul, L. Moscou, R. A. Pierotti, J. Rouquérol, T. Siemieniewska, *Pure Appl. Chem.* **1985**, *57*, 603–619.
[85] S. J. Gregg, K. S. W. Sing, *Adsorption, Surface Area and Porosity*, Academic Press, New York, **1982**.
[86] E. Barrett, L. G. Joyner, P. P. Halenda, *J. Am. Chem. Soc.* **1951**, *73*, 373–380.
[87] S. Fujita, S. Inagaki, *Chem. Mater.* **2008**, *20*, 891–908.
[88] G. Cerveau, R. J. P. Corriu, E. Framery, F. Lerouge, *J. Mater. Chem.* **2004**, *14*, 3019–3025.
[89] J. J. E. Moreau, L. Vellutini, M. W. Chi Man, C. Bied, P. Dieudonné, J.-L. Bantignies, J.-L. Sauvajol, *Chem. Eur. J.* **2005**, *11*, 1527–1537.
[90] F. Lerouge, G. Cerveau, R. J. P. Corriu, *New J. Chem.* **2006**, *30*, 1364–1376.
[91] J.-L. Bantignies, L. Vellutini, D. Maurin, P. Hermet, P. Dieudonné, M. Wong Chi Man, J. R. Bartlett, C. Bied, J.-L. Sauvajol, J. J. E. Moreau, *J. Phys. Chem. B* **2006**, *110*, 15797–15802.
[92] J. Alauzun, A. Mehdi, C. Reyé, R. J. P. Corriu, *Chem. Commun.* **2006**, 347–349.
[93] Y. Kaneko, N. Iyi, K. Kurashima, T. Matsumoto, T. Fujita, K. Kitamura, *Chem. Mater.* **2004**, *16*, 3417–3423.
[94] A. Shimojima, Z. Liu, T. Ohsuna, O. Terasaki, K. Kuroda, *J. Am. Chem. Soc.* **2005**, *127*, 14108–14116.
[95] K. Okamoto, G. Y. S. Inagaki, *J. Mater. Chem.* **2005**, *15*, 4136–4140.
[96] R. Mouawia, A. Mehdi, C. Reye, R. J. P. Corriu, *J. Mater. Chem.* **2008**, *18*, 2028–2035.
[97] F. Lerouge, G. Cerveau, R. J. P. Corriu, *New J. Chem.* **2006**, *30*, 272–276.
[98] R. S. Drago, C. E. Webster, J. M. McGilvray, *J. Am. Chem. Soc.* **1998**, *120*, 538–547.
[99] C. E. Webster, A. Cottone III, R. S. Drago, *J. Am. Chem. Soc.* **1999**, *121*, 12127–12139.
[100] C. E. Webster, R. S. Drago, *Microporous Mesoporous Mater.* **1999**, *33*, 291–306.
[101] E. Besson, A. Mehdi, D. A. Lerner, C. Reyé, R. J. P. Corriu, *J. Mater. Chem.* **2005**, *15*, 803–809.
[102] B. Boury, R. J. P. Corriu, P. Delord, V. Le Strat, *J. Non-Cryst. Solids* **2000**, *265*, 41–50.
[103] D. Reinen, C. Friebel, *Inorg. Chem.* **1984**, *23*, 791–798.
[104] S. Alvarez, M. Llunell, *J. Chem. Soc. Dalton Trans.* **2000**, 3288–3303.
[105] D. Maiti, D.-H. Lee, K. Gaoutchenova, C. Würtele, M. C. Holthausen, A. A. Narducci Sarjeant, J. Sundermeyer, S. Schindler, K. D. Karlin, *Angew. Chem.* **2008**, *120*, 88–91; *Angew. Chem. Int. Ed.* **2008**, *47*, 82–85.
[106] A. G. Blackman, *Polyhedron* **2005**, *24*, 1–39.

[107] G. A. McLachlan, G. D. Fallon, R. L. Martin, L. Spiccia, *Inorg. Chem.* **1995**, *34*, 254–261.
[108] F. Thaler, C. D. Hubbard, F. W. Heinemann, R. Van Eldik, S. Schindler, I. Fabian, A. M. Dittler-Klingemann, F. E. Hahn, C. Orvig, *Inorg. Chem.* **1998**, *37*, 4022–4029.
[109] B. J. Hathaway, D. E. Billing, *Coord. Chem. Rev.* **1970**, *5*, 143–207.
[110] R. Barbucci, A. Bencini, D. Gatteschi, *Inorg. Chem.* **1977**, *16*, 2117–2120.
[111] M. Duggan, N. Ray, B. Hathaway, G. Tomlinson, P. Brint, K. Pelin, *J. Chem. Soc. Dalton* **1980**, 1342–1348.
[112] E. V. Rybak-Akimova, A. Y. Nazarenko, L. Chen, P. W. Krieger, A. M. Herrera, V. V. Tarasov, P. D. Robinson, *Inorg. Chim. Acta* **2001**, *324*, 1–15.
[113] Y. Dong, G. A. Lawrance, L. F. Lindoy, P. Turner, *Dalton Trans.* **2003**, 1567–1576.
[114] A. Almesaker, P. Gamez, J. Reedijk, J. L. Scott, L. Spiccia, S. J. Teat, *Dalton Trans.* **2009**, 4077–4080.
[115] A. J. Fischmann, A. C. Warden, J. Black, L. Spiccia, *Inorg. Chem.* **2004**, *43*, 6568–6578.
[116] J. R. Pilbrow, *Transition Ion Electron Paramagnetic Resonance*, 1st ed., Clarendon Press, Oxford, **1990**.
[117] S. Torelli, C. Belle, I. Gautier-Luneau, J.-L. Pierre, E. Saint-Aman, J.-M. Latour, L. Le Pape, D. Luneau, *Inorg. Chem.* **2000**, *39*, 3526–3536.
[118] S. Torelli, C. Belle, S. Hamman, J.-L. Pierre, *Inorg. Chem.* **2002**, *41*, 3983–3989.
[119] D. Maiti, H. C. Fry, J. S. Woertink, M. A. Vance, E. I. Solomon, K. D. Karlin, *J. Am. Chem. Soc.* **2007**, *129*, 264–265.
[120] S. C. Larsen, A. Aylor, A. T. Bell, J. A. Reimer, *J. Phys. Chem.* **1994**, *98*, 11533–11540.
[121] G. T. Palomino, P. Fisicaro, S. Bordiga, A. Zecchina, E. Giamello, C. Lamberti, *J. Phys. Chem. B* **2000**, *104*, 4064–4073.
[122] S. Recchia, C. Dossi, R. Psaro, A. Fusi, R. Ugo, G. Moretti, *J. Phys. Chem. B* **2002**, *106*, 13326–13332.
[123] M. H. Groothaert, J. A. Van Bokhoven, A. A. Battiston, B. M. Weckhuysen, R. A. Schoonheydt, *J. Am. Chem. Soc.* **2003**, *125*, 7629–7640.
[124] A. Itadani, M. Tanaka, Y. Kuroda, M. Nagao, *New J. Chem.* **2007**, *31*, 1681–1690.
[125] S. Itoh, Y. Tachi, *Dalton Trans.* **2006**, 4531–4538.
[126] C. X. Zhang, H.-C. Liang, E. Kim, J. Shearer, M. E. Helton, E. Kim, S. Kaderli, C. D. Incarvito, A. D. Zuberbühler, A. L. Rheingold, K. D. Karlin, *J. Am. Chem. Soc.* **2003**, *125*, 634–635.
[127] M. Schatz, M. Leibold, S. P. Foxon, M. Weitzer, F. W. Heinemann, F. Hampel, O. Walter, S. Schindler, *Dalton Trans.* **2003**, 1480–1487.
[128] S. Itoh, *Curr. Opin. Chem. Biol.* **2006**, *10*, 115–122.
[129] J. Alauzun, A. Mehdi, C. Reyé, R. J. P. Corriu, *J. Mater. Chem.* **2005**, *15*, 841–843.
[130] S. Brunauer, P. H. Emmet, E. Teller, *J. Am. Chem. Soc.* **1938**, *60*, 309–319.

Received: November 17, 2009
Revised: January 27, 2010
Published online: April 16, 2010

